

A six-degrees-of-freedom platform for deci-hertz active isolation using optical inertial sensors

Journal of Low Frequency Noise,
Vibration and Active Control
2025, Vol. 0(0) 1–13
© The Author(s) 2025
DOI: 10.1177/14613484251342629
journals.sagepub.com/home/lfn



Mouhamad Haidar Lakkis^{1,2} , Jennifer Watchi², Rasa Jamshidi¹, Ameer Sider¹, Anthony Amorosi^{1,2} and Christophe Collette^{1,2}

Abstract

This paper addresses a theoretical control approach and its corresponding experimental validation for low-frequency active damping and isolation of a six-degree-of-freedom platform using high-resolution inertial sensors. Six vacuum-operating inertial sensors are placed on top of the platform to actively control it. Three of them measure displacements in horizontal directions and three in vertical directions. The resonance frequencies of the vertical and horizontal sensors range between 0.3 and 0.7 Hz with a resolution of $2 \times 10^{-13} \text{ m}/\sqrt{\text{Hz}}$ at 1 Hz for both types of sensors. Sensor signals are fed back into six voice coil actuators (three horizontal and three vertical) mounted below the platform. Actuators and sensors are placed in a quasi-collocated architecture facilitating the controllability of the plant. The platform (with resonance frequencies ranging between 1 and 10 Hz) is actively isolated by up to two orders of magnitude between 0.1 and 10 Hz, yielding a final overall displacement RMS value below 100 nm at its center of mass from 0.3 Hz onward.

Keywords

active vibration isolation, low frequency, six degrees of freedom, optical inertial sensors, MIMO control system

Introduction

After the first detection of gravitational waves in 2015,^{1,2} a new era in understanding the universe began. To make such detection possible, gravitational wave detectors are required to operate in an ultrastable environment that can only be obtained by isolating them from external disturbances. Active isolation control is a major approach in this context as it was successfully implemented in LIGO's (Laser Interferometer Gravitational-Wave Observatory) positioning platform,^{3,4} where it is possible to obtain amplitude spectral densities lower than $10^{-12} \text{ m}/\sqrt{\text{Hz}}$ for vertical and longitudinal seismic isolation at frequencies higher than 1 Hz. It is still extremely challenging to obtain such good performance at lower frequencies, where noise sources such as seismic motion are more dominant. Nevertheless, pushing future detectors' sensitivity at lower frequencies is essential to boost their performances and enable the detection of an even wider range of gravitational waves.⁵

To the best of the authors' knowledge, all six-degrees-of-freedom active vibration isolation platforms that operate effectively at low frequencies (particularly below 1 Hz) rely on relative displacement sensors in alongside inertial sensors. This approach is standard in high-end systems such as the Advanced LIGO seismic isolation platforms,⁴ and the AEI-SAS platform,⁶ all of which use capacitive or optical displacement sensors to measure relative motion between the isolated

¹Department of Aerospace and Mechanical Engineering, Université de Liège, Liege, Belgium

²BEAMS Department, Université libre de Bruxelles, Brussels, Belgium

Corresponding author:

M. Haidar Lakkis, Department of Aerospace and Mechanical Engineering, Université de Liège, Pl. du Vingt Août 7, Liege 4000, Belgium.

Email: mhlakkis@uliege.be



Creative Commons CC BY: This article is distributed under the terms of the Creative Commons Attribution 4.0 License (<https://creativecommons.org/licenses/by/4.0/>) which permits any use, reproduction and distribution of the work without further permission provided the original work is attributed as specified on the SAGE and Open Access pages (<https://us.sagepub.com/en-us/nam/open-access-at-sage>).

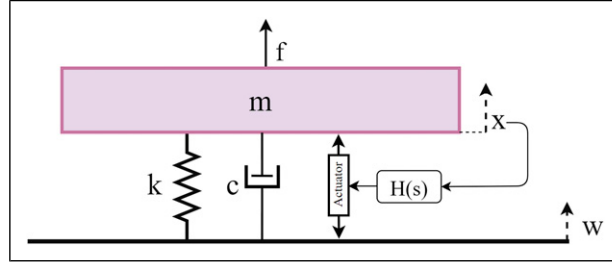


Figure 1. Sketch showing the principle of an inertial control for one-degree-of-freedom system. $H(s)$ is a controller used to feedback the absolute displacement of a mass m to an actuator to actively isolate it from external force disturbances f and transmitted ground motion w .

payload and the base. These measurements are essential not only to overcome the poor signal-to-noise ratio and high $1/f$ noise of inertial sensors at low frequencies but also to mitigate the effects of tilt-horizontal coupling, a well-known limitation in horizontal inertial sensors. Furthermore, these platforms typically implement control loops in the Cartesian frame, where sensor signals are transformed into global translational and rotational degrees of freedom. By combining inertial sensors for mid- to high-frequency control with relative displacement sensors for low-frequency feedback, these platforms achieve broadband isolation with high stability. In contrast, the main difference in this platform is that it is (1) investigating active isolation using only optical inertial sensors with (2) a decentralized collocated approach for closing the control loops. (3) Compared to existing platforms, the isolation system proposed in this paper is also modular by design, which means that it can easily accommodate a large variety of payloads.

The following sections of this paper discuss the concept of inertial control (precision control approach used for active isolation and disturbance rejection) for a one-degree-of-freedom system, followed by the working principle of inertial sensors, sensors used to isolate the six-degrees-of-freedom platform and their resolution. Then modeling, model tuning of the six-degrees-of-freedom platform and its correlation with the experimental data are discussed. Then the MIMO (Multiple-Input Multiple-Output) inertial control approach that is used to isolate the platform in all six degrees of freedom is introduced, and finally, the last two sections introduce experimental performances and practical limitations of the active isolation of the platform.

Inertial control

Active inertial control is a feedback control concept that is widely used in instrument isolation applications.⁷ To exemplify it, consider a one-degree-of-freedom system where a mass m is connected to a spring with stiffness k , a damper with damping constant c , and an actuator that applies a force equal to a defined input command (Figure 1).

Two external disturbances, f denoting external forces applied on m and w denoting the displacement of the ground induce an undesirable displacement x of the payload mass m . By deriving the equations of motion, it is possible to get the transfer function from external disturbance force f to mass displacement x (compliance transfer function) and the transfer function from ground motion w to mass displacement x (transmissibility transfer function):

$$T_{fx}(s) = \frac{x(s)}{f(s)} = \frac{1}{ms^2 + cs + k} \quad (1)$$

$$T_{wx}(s) = \frac{x(s)}{w(s)} = \frac{cs + k}{ms^2 + cs + k} \quad (2)$$

Active inertial isolation is based on feeding back the absolute displacement x of m into the actuators so that the actuator applies a force in the opposite direction of x and pushes it to lower values. Moreover, when including a feedback controller $H(S)$ and deriving the equations of motion, closed-loop compliance and transmissibility transfer functions can be written as:

$$T_{fx}(s) = \frac{x(s)}{f(s)} = \frac{1}{ms^2 + cs + k + H(s)} \quad (3)$$

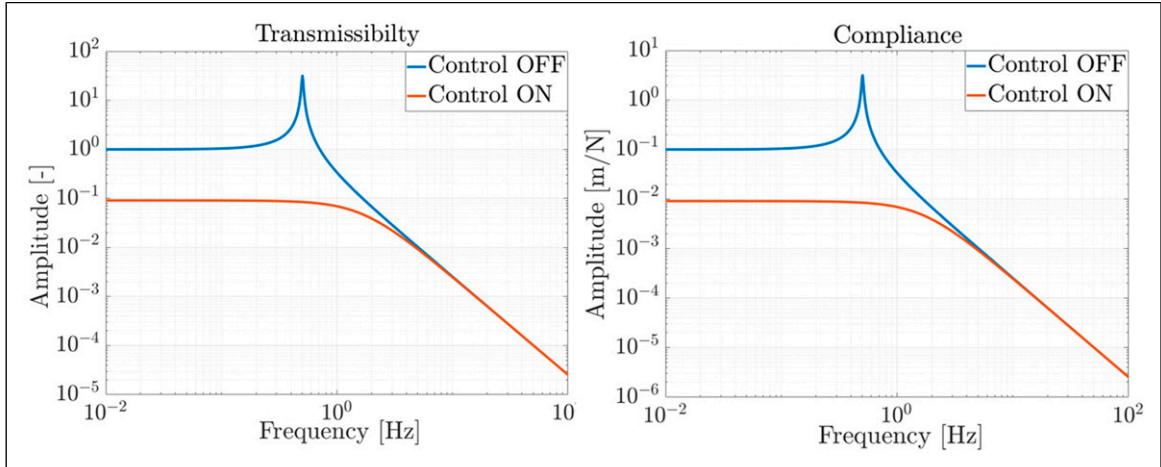


Figure 2. Magnitude of transfer functions from ground motion \mathbf{w} to displacement \mathbf{x} (left) and magnitude of transfer functions from external force disturbance \mathbf{f} to displacement \mathbf{x} (right) for inertial control off (in blue) and inertial control on (in red).

$$T_{wx}(s) = \frac{x(s)}{w(s)} = \frac{cs + k}{ms^2 + cs + k + H(s)} \quad (4)$$

Equations (3) and (4) imply that the closed-loop transmissibility and compliance transfer functions converge to zero as the controller gain tends to infinity. So, when applying controllers with high gains, the payload is less sensitive to external force disturbances and transmitted ground motion, and consequently, the payload is isolated from these disturbances.

The transfer function from actuation force to displacement x of the one-degree-of-freedom system (Figure 1) constitutes a pair of complex poles and a phase starting around 0° before the resonance frequency and converging to 180° at high frequencies. So, a proportional derivative controller is a reasonable choice to ensure high loop gain before the resonance while guaranteeing a good phase margin because of the phase lead introduced by the derivative term around the crossover frequency. Taking into account, for example, the parameters $m = 1$ kg, $k = 10$ N/m and $c = 0.1$ Ns/m, the following PD controller is used:

$$H(s) = 100 + 20s \quad (5)$$

Closing the loop using Eq. (5) facilitates damping the system's resonance at 0.5 Hz and isolating the payload for one order of magnitude between frequency response at $s = 0$ (DC) and the vicinity of the system's resonance (Figure 2).

This implies that with inertial control, the mass m is ten times less sensitive to external force excitation or ground motion for frequencies between DC and 1 Hz. However, it is not straightforward to measure low-frequency absolute displacement x , so optical inertial sensors are used to approximate it. The concept of these sensors and their resolution are presented in the following section.

Optical inertial sensor

Inertial sensors are one-degree-of-freedom oscillators that return the relative displacement between the sensor's base and an oscillating mass as an output. Assuming a simple inertial sensor that has a mass m_{IS} , stiffness k_{IS} , and damping constant c_{IS} as shown in Figure 3, and by deriving the equations of motion, it is possible to write the sensitivity transfer function from the absolute displacement of the base of the inertial sensor $x(s)$ to the output of the inertial sensor $y_{IS}(s)$ as follows⁸:

$$T_{xy}(s) = \frac{y_{IS}(s)}{x(s)} = \frac{-m_{IS}s^2}{m_{IS}s^2 + c_{IS}s + k_{IS}} \quad (6)$$

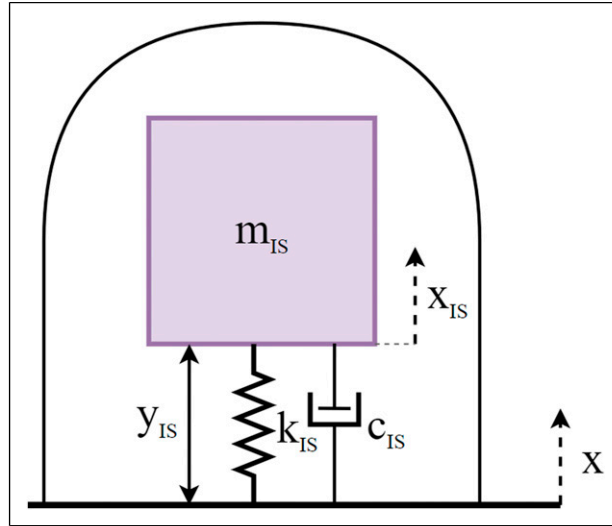


Figure 3. Sketch showing the principle of an inertial sensor. y_{IS} is the output of the sensor where it is an approximation of the absolute displacement x_{IS} of the surface where the sensor is placed.

The sensitivity transfer function shows that for frequencies higher than the sensor's resonance frequency ($\sqrt{k_{IS}/m_{IS}}$) its magnitude tends to one. This means that the relative displacement between the base of the sensor and the mass m gives a good measurement of the displacement x . However, for frequencies lower than the sensor's resonance frequency, the output of the sensor is proportional to the acceleration on the base.

To actively isolate the six-degrees-of-freedom platform, an optical horizontal inertial sensor (HINS) and an optical vertical inertial sensor (VINS) were studied and developed in Ref. 9. These inertial sensors are one-degree-of-freedom pendulums where an interferometric readout is deployed to measure the relative mass displacement. In this particular case of HINS and VINS, Michelson interferometric readouts are used to ensure a resolution of around 10^{-12} m/ $\sqrt{\text{Hz}}$ at 1 Hz (Figure 4).

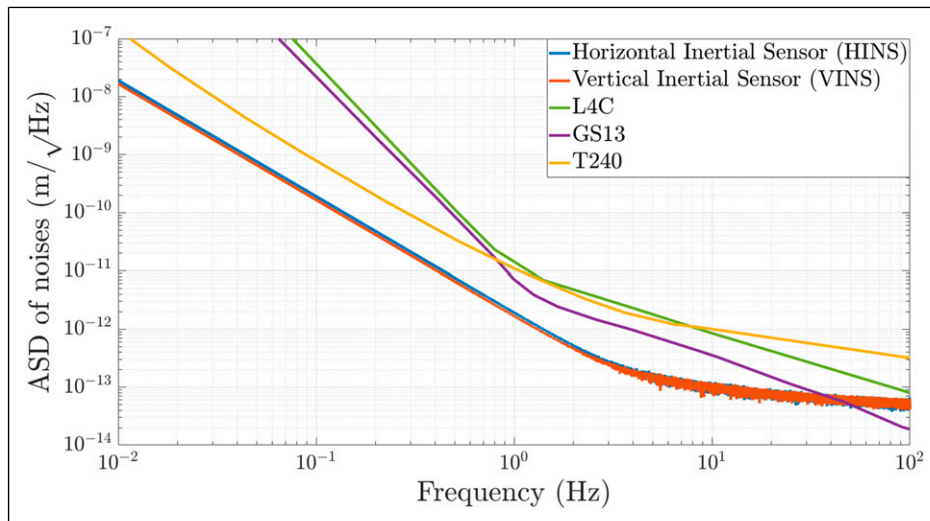


Figure 4. Resolution of the horizontal inertial sensor (HINS) and the vertical inertial sensor (VINS). The resolution of most common and commercial use sensors such as L4C, GS13, and T240 are plotted for comparison.

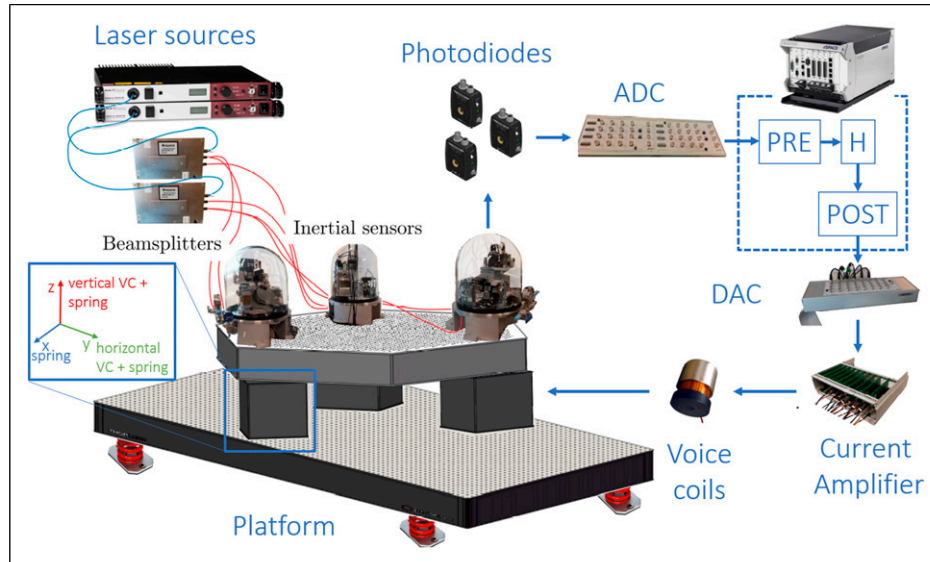


Figure 5. Experimental setup of the platform (hexagonal-shaped table). Two laser sources feed the inertial sensors using optical fibers and two beam splitters. Each sensor has an interferometric readout that returns the voltage of three photodiodes as an output. Photodiodes signals are passed through an analog-digital converter and demodulated in real time to give the displacement measured by each sensor. These signals are multiplied by a controller matrix and passed through a digital-analog converter to give the control command which is fed to a current amplifier that drives six voice coil actuators (in black boxes). The platform is placed on a passive isolation stage (rectangular table).

Six-degrees-of-freedom platform

The payload to be isolated is a hexagonal-shaped platform. It is placed on three vertical and three horizontal springs that are mounted on top of a passively isolated rectangular stage (Figure 5). On top of the platform, vacuum chambers are mounted, each one containing a horizontal inertial sensor and a vertical inertial sensor. Two laser sources and two beam splitters alongside optical fibers are used to feed the six inertial sensors with laser beams at 1550 nm wavelength and 5 mW power per sensor. The interferometric readout includes three photodiodes, and their signals are passed through an analog-digital converter and further processed using a demodulation algorithm. This algorithm gives the output of the relative displacement of the inertial sensor in real time.⁹ Six voice coil actuators are mounted between the passive stage and the platform to allow actuation on the bottom face of the platform. They are placed in a quasi-collocated manner with the sensors to ensure alternating complex poles and zeros in the transfer functions from actuators to inertial sensors and hence facilitate the control of the system.¹⁰

Furthermore, the actuators and springs of the platform are perfectly collocated with each other (both inside the three black boxes shown in Figure 5). The actuator architecture can be shown in the sketch in Figure 6 where every vertical actuator coincides with a horizontal one and the three pairs of horizontal actuator-vertical actuators are placed and oriented in a way that corresponds to a third-order rotational symmetry. Inertial sensors that are placed on top of the active platform are oriented in the same direction as the actuators.

A multibody system model was built using SimscapeTM.¹¹ Each sensor is modeled as a one-degree-of-freedom oscillator whose output is the relative displacement between the active platform and its proof mass. The actuators, springs, and damping elements are then defined on the bottom face of the active stage as point elements with stiffness, damping ratios, and defined input force (Figure 7).

The nature of the platform yields a highly coupled multiple-input multiple-output system with a fully populated transfer matrix, as each sensor is sensitive to excitation induced by all six actuators. Hence, multibody dynamic modeling facilitates the understanding of these couplings, their nature, and the parameters governing them. Some parameters used in modeling this system can be found in Table 1.

Model-experimental open loop transfer functions from each actuator to its collocated sensor comparison is shown in Figure 8 for horizontal loops and Figure 9 for vertical loops. Resonances of the horizontal and vertical inertial sensors are popping out around 0.2–0.3 Hz followed by the rigid body modes of the active platform between 0.8 and 5 Hz. The model sufficiently matches the experiment from 0.1 Hz above, however, this matching drops at lower

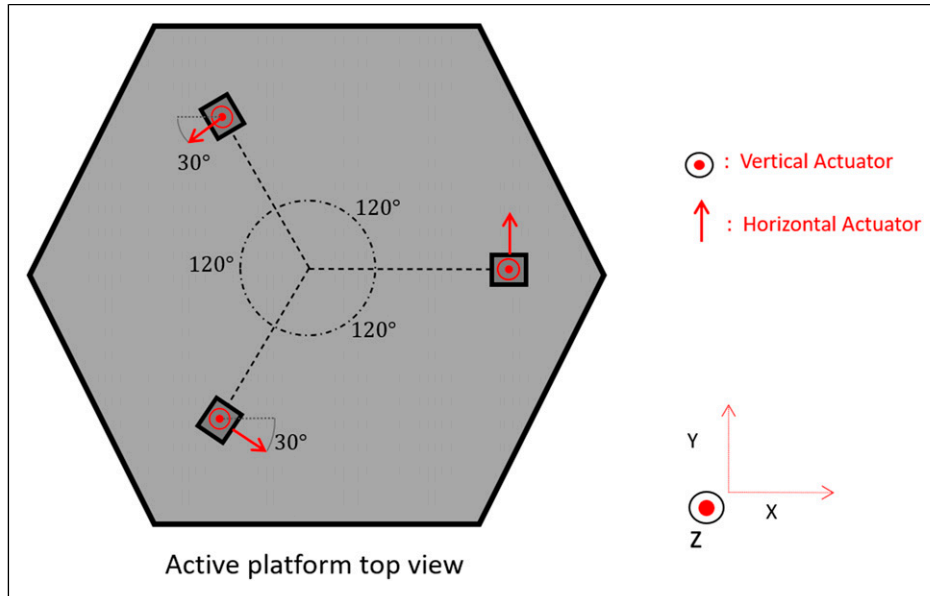


Figure 6. Sketch showing actuators' positions and directions on the active platform. The orientations of the horizontal actuators are 120° shifted from each other to facilitate actuation in X and Y directions. Vertical actuators have the same orientation, allowing them to actuate in Z direction. All six actuators are placed away from the center of mass to allow applying moments around the three axes.

frequencies due to the tilt-horizontal coupling problem (check section) where it is not straightforward to anticipate this coupling behavior using multibody system modeling.

Control approach

A decentralized control approach is considered to actively isolate the platform. The signal from each inertial sensor passes through a controller and is fed back to its quasi-collocated voice coil actuator, as shown in Figure 10.

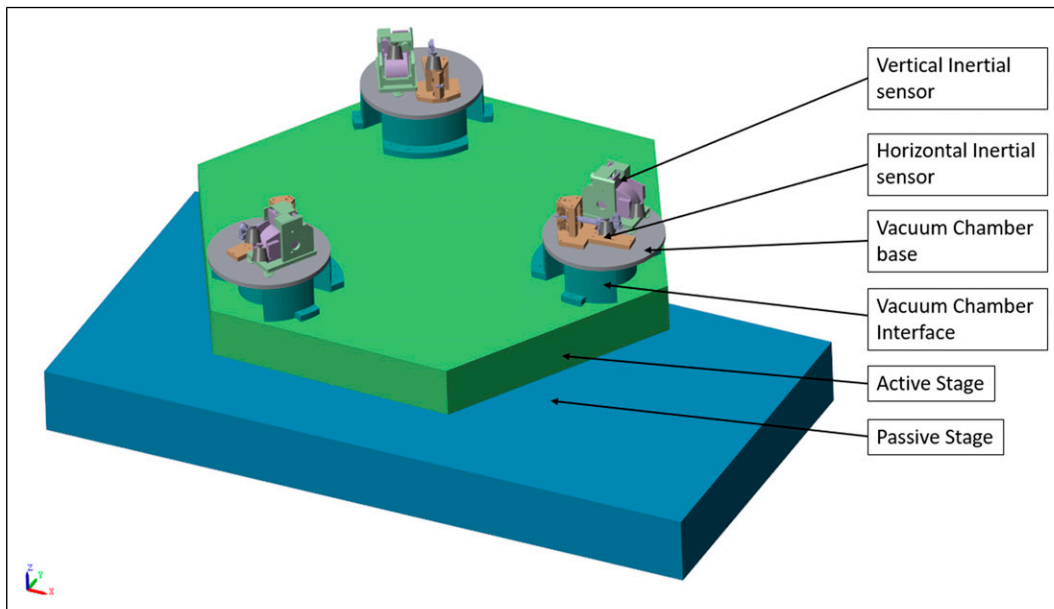


Figure 7. CAD view of the Simscape™ model of the six-degrees-of-freedom platform.

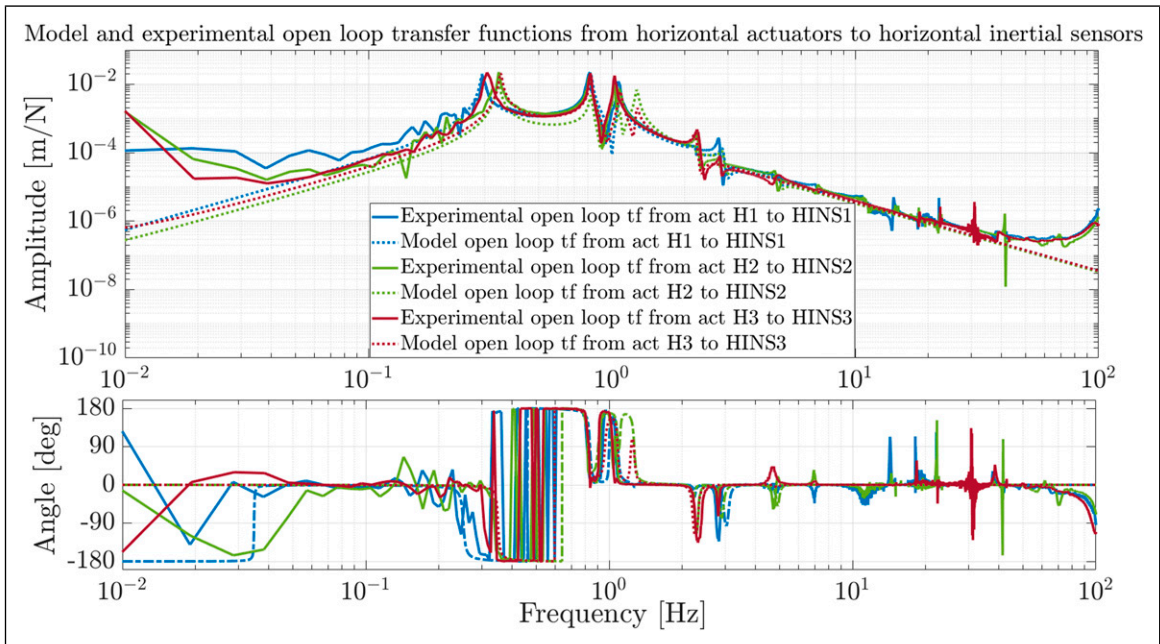
Table 1. Table showing stiffness and mass parameters used in modeling the platform.

Parameter	Value	Description
Horizontal stiffness (in kN/m)	$k_{h1} = 7.35$ $k_{h2} = 5.75$ $k_{h3} = 2.5$	Horizontal stiffness of the three horizontal springs in the directions of the horizontal actuators
Tangential stiffness (in kN/m)	$k_{h1t} = 8$ $k_{h2t} = 5.75$ $k_{h3t} = 2.5$	Horizontal stiffness of the three horizontal springs in the tangential directions of the horizontal actuators
Vertical stiffness (in kN/m)	$k_{v1} = 25.55$ $k_{v2} = 20.07$ $k_{h3t} = 3.164$	Vertical stiffness of the three vertical springs in the directions of the vertical actuators
Masses (in kg)	$m_{Hexagonal} = 153$ $m_{sensor+vacuum} = 34$ $m_{total} = 255$ $m_{passive} = 250$	Masses of the hexagonal table, each sensor module (including one horizontal and one vertical sensor alongside with vacuum chamber base and glass bell), the total mass of the active platform + sensor modules, and finally the mass of the passive stage

Since the sensor-actuator architecture corresponds to a third-degree rotational symmetry architecture the six diagonal transfer functions can be described using two open loops, the open loop from a horizontal actuator to a collocated horizontal sensor is denoted as a horizontal loop and the open loop from a vertical actuator to a collocated vertical sensor is denoted as a vertical loop. Then, two lead-lag controllers are designed and implemented experimentally to close horizontal and vertical loops as in (7) and (8) respectively:

$$C_H = 10^6 \frac{50 \times 0.005 (s + 2\pi 0.7)(s + 2\pi 0.7)}{0.7 \times 0.7 (s + 2\pi 50)(s + 2\pi 0.005)} \quad (7)$$

$$C_V = -3.7 \times 10^6 \frac{(s + 2\pi 0.2)(s + 2\pi 9)(s + 2\pi 9)}{(s + 2\pi 30)(s + 2\pi 40)(s + 2\pi 0.005)} \quad (8)$$

**Figure 8.** Bode plots of modeled transfer functions (in dotted lines) and experimental transfer functions (in solid lines) from horizontal actuators to horizontal inertial sensors.

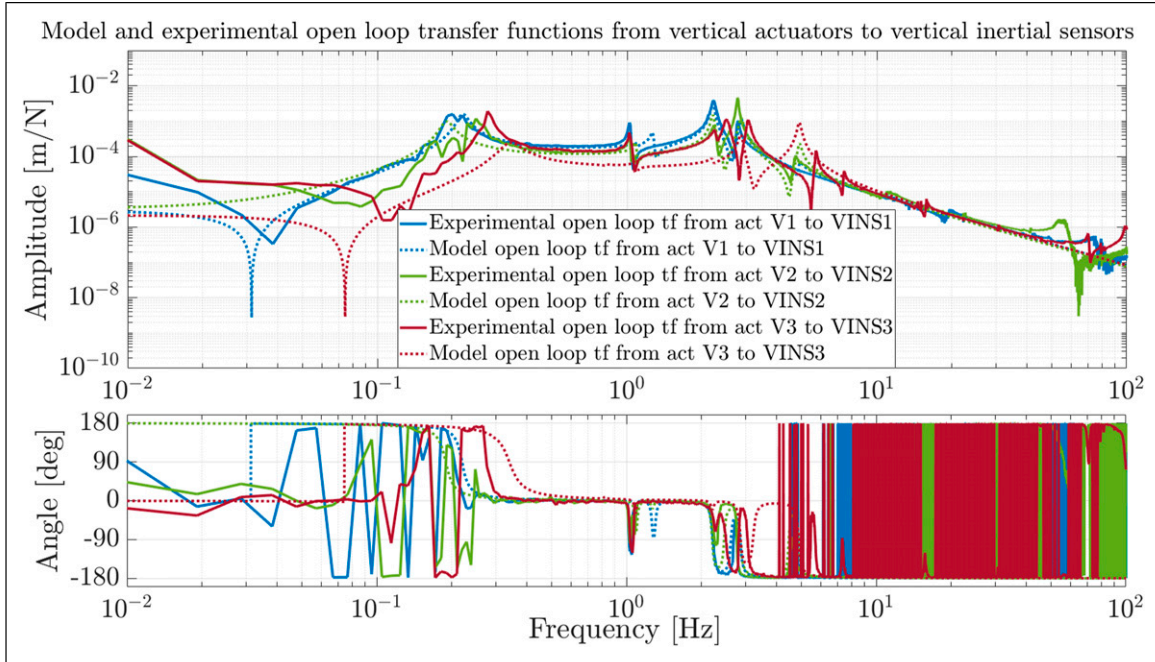


Figure 9. Bode plots of modeled transfer functions (in dotted lines) and experimental transfer functions (in solid lines) from vertical actuators to vertical inertial sensors.

The Bode plots of these controllers can be shown in [Figure 11](#) multiplied by a first-order high-pass filter with a corner frequency of 50 mHz to avoid actuator saturation and a second-order low-pass filter with a corner frequency of 50 Hz to diminish the impact of flexible modes after 100 Hz.

Moreover, since the system is highly coupled, sequential loop closing is used to design controllers while guaranteeing MIMO stability.¹² The coupling in the plant can be visualized using the block diagram in [Figure 12](#).

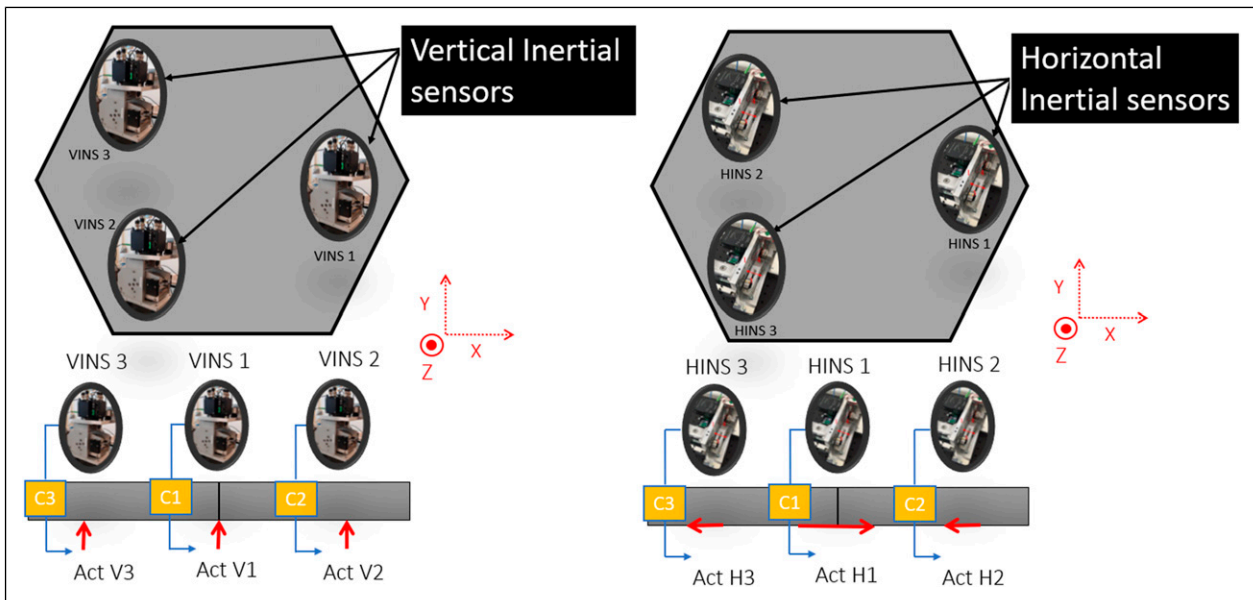


Figure 10. Sketch showing decentralized control architecture for the six-degrees-of-freedom system.

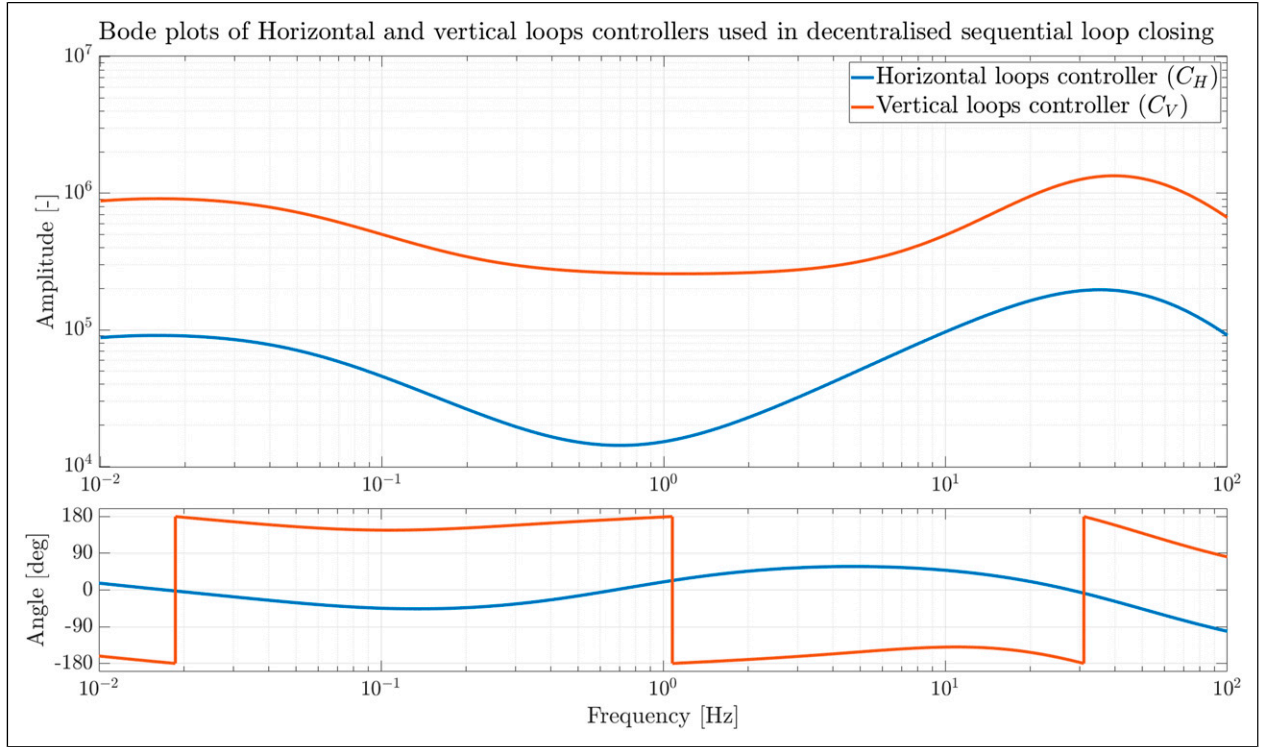


Figure 11. Bode plot of horizontal and vertical controllers used in decentralized sequential loop closing.

Sequential loop design simplifies MIMO stability by assessing sub-systems' stability with fewer inputs and outputs. In the case of the platform, stability could be guaranteed by first designing a 3×3 controller C_V while ensuring that it stabilizes G_{vv} , this yields an equivalent G_{hh}^{eq} (Figure 12), and then designing a 3×3 controller C_H while ensuring that it stabilizes G_{hh}^{eq} .

Moreover, after applying sequential loop closing for the first time, the system's stability is dependent on two 3×3 MIMO systems. The stability of each of them is then assessed using sequential loop closing again while ensuring identical controllers for the three horizontal loops and the three vertical loops.

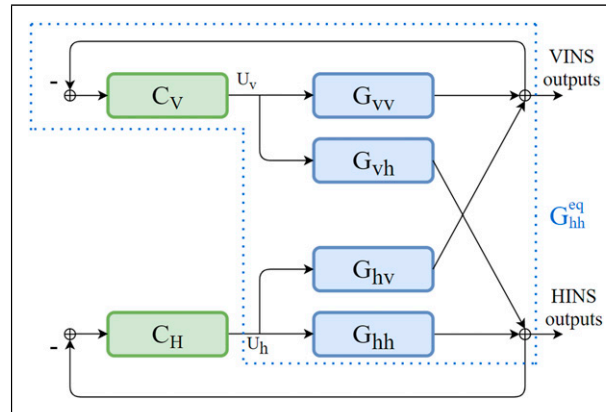


Figure 12. Block diagram showing subsystems and controllers where G_{vv} is the subsystem with three vertical actuators as inputs and three vertical inertial sensors as outputs, G_{hh} is the subsystem with three horizontal actuators as inputs and three horizontal inertial sensors as outputs, G_{vh} is the subsystem with three vertical actuators as inputs and three horizontal inertial sensors as outputs, and G_{hv} is the subsystem with three horizontal actuators as inputs and three vertical inertial sensors as outputs. C_V and C_H are 3×3 diagonal control matrices containing C_v and C_h , respectively, as diagonal elements.

Experimental results

Outputs of the six inertial sensors are multiplied by their inverse dynamics and then by decoupling matrices to reconstruct sensing in Cartesian coordinates at the center of mass of the platform. The amplitude spectral densities for control off and control on between 100 mHz and 10 Hz in X, Y, and θ_z directions are shown in Figure 13 (RMS value in Figure 17). Isolation in these three directions comes from closing the loops from horizontal actuators to the corresponding quasi-collocated horizontal inertial sensors. We obtained around half to one order of magnitude of isolation between 300 mHz and 3 Hz. Performance limitations in these degrees of freedom come from the translation-rotation coupling problem of inertial sensors which is more significant in horizontal sensors.

Moreover, the translation-rotation coupling is less critical for vertical inertial sensors allowing to apply more gains when closing loops from vertical actuators to corresponding collocated vertical inertial sensors. This allows more isolation in the remaining degrees of freedom Z, θ_{α_x} and θ_{α_y} . In these three directions, the platform is actively isolated between 100 mHz and 10 Hz up to two orders of magnitude, as shown in Figure 14 (RMS value in Figure 16).

By placing a Guralp 6T seismometer on the ground, it was possible to check the transmissibility transfer functions from the ground displacement in the three translational directions to the platform displacement in the three translational directions. They can be shown in Figure 15. The order of isolation shown in the transmissibilities is similar to what is shown for the ASDs in X, Y, and Z translational directions, consolidating the obtained isolation level.

Practical limitations

Some practical limitations of the isolation level of the platform are:

- Tilt-horizontal actuation coupling:** When trying to actuate the platform in a horizontal translation direction, the platform is translated and tilted at the same time, which means that the platform is following an arc trajectory instead of a straight line. This kind of actuation induces non-minimum phase zeros in control transfer functions with frequencies proportional to the inverse of the square root of the radius of curvature of the trajectory arc.¹³ These zeros are a major control limitation that compromises stability and could cause displacement amplifications at low frequencies (see Figure 13 around 0.1–0.2 Hz). To overcome this limitation, we plan on adding optical levers^{14,15} and relative displacement sensors to give a better measure of rotation and translation and further facilitate decoupling them.

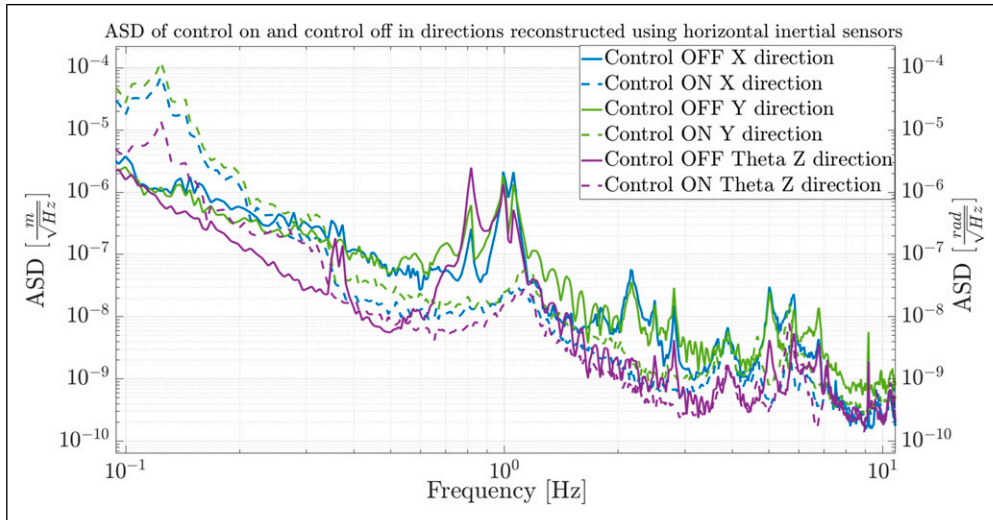


Figure 13. Amplitude spectral densities of displacements measured in X, Y, and θ_z directions on top of the platform for control off (solid lines) and control on (dashed lines).

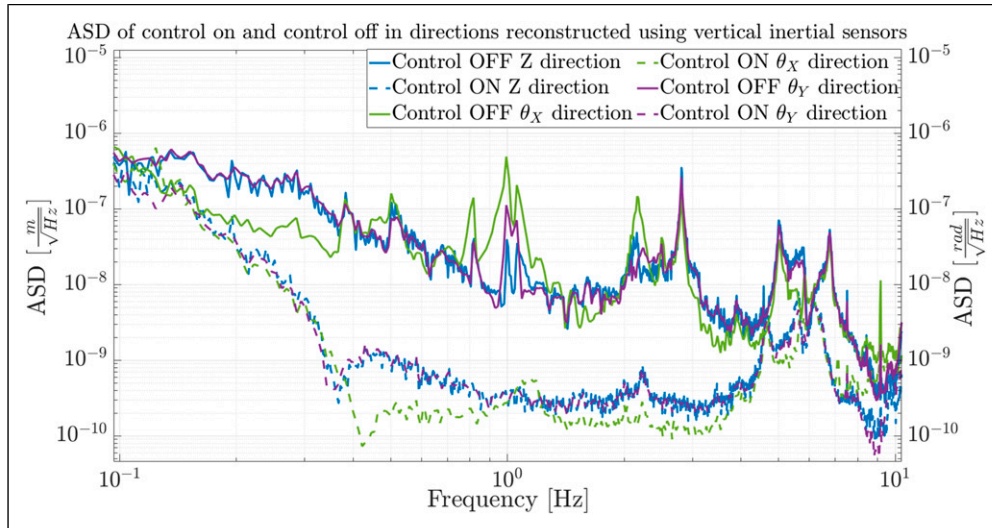


Figure 14. Amplitude spectral densities of displacements measured in Z, θ_x , and θ_y directions on top of the platform for control off (solid lines) and control on (dashed lines).

- **Flexible modes:** Flexible modes of the platform appearing at frequencies above 100 Hz are limiting the gain and phase margins of the closed-loop system. To deal with that, MIMO virtual sensor fusion will be applied at high frequencies to push gains further while ensuring stability in the vicinity of flexible mode frequencies.
- **Components alignment:** Low tolerances between coils and magnets of the used voice coil actuators alongside the displacement of the slightly damped platform when the control is off made coils and magnets of the actuators touch. Hence, this induced friction in the system. To deal with that, the actuators had to be placed accurately and calibrated to ensure that the load is distributed equally and consequently none of the voice coils are touching.

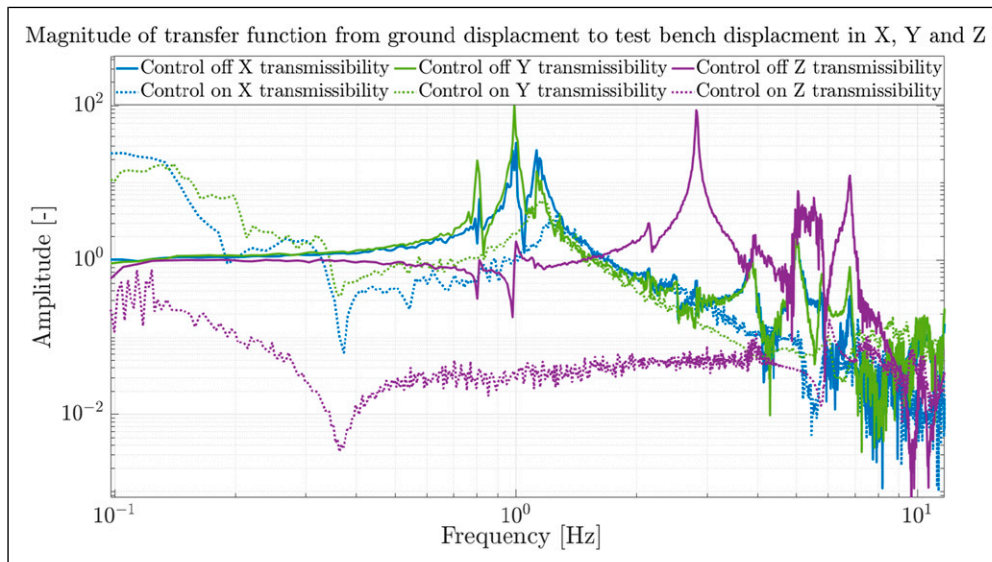


Figure 15. Figure showing the magnitude of the ground to active platform transmissibility transfer function for control off (solid lines) and control on (dotted lines) in X (in blue), Y (in dark green), and Z (in purple) directions.

- **Stiffness mismatch:** As stated in the in section, the platform should correspond to a third-degree cyclic symmetry. However, the stiffness of the platform springs is mismatched (Table 1) which leads to some loss in the system's symmetry.

Conclusion

This paper presented a six-degree-of-freedom platform dedicated to low-frequency seismic isolation of instruments requiring high precision. To the best of the author's knowledge, this is the first platform fully controlled by interferometric inertial sensors. The platform was actively isolated in the vertical direction (Z) and rotational directions around the two horizontal axes (θ_X, θ_Y) between half and two orders of magnitude for frequencies between 100 mHz and 10 Hz. However, this isolation dropped down in the two horizontal directions (X, Y) and rotational direction around the vertical axis (θ_Z) where it was isolated by half an order of magnitude between 300 mHz and 3 Hz.

Acknowledgments

The authors gratefully acknowledge the European Research Council, Consolidator grant SILENT (grant agreement number 866259) for funding this research and the French Community as part of the financing of a FRIA grant for Jennifer Watchi (grant number: FC 27289). The authors also acknowledge the LIGO scientific community for reviewing this research. This paper has been assigned the LIGO DCC number LIGO-P2400052.

ORCID iD

Mouhamad Haidar Lakkis  <https://orcid.org/0000-0002-1754-5969>

Funding

The author(s) disclosed receipt of the following financial support for the research, authorship, and/or publication of this article: H2020 European Research Council (866259).

Declaration of conflicting interests

The author(s) declared no potential conflicts of interest with respect to the research, authorship, and/or publication of this article.

References

1. Abbott B. Observation of Gravitational Waves from a Binary Black Hole Merger. *Physical Review Letters* 2016; 2: 061102.
2. Castelvevchi D and Witze A. Gravitational waves found at last. *Nature* 2016; 2. doi:10.1038/nature.2016.19361.
3. Matichard F, Abbott B, Abbott S, et al. Advanced LIGO two-stage twelve-axis vibration isolation and positioning platform. Part 1: design and production overview. *Precis Eng* 2015; 40: 273–286.
4. Matichard F, Abbott B, Abbott S, et al. Advanced LIGO two-stage twelve-axis vibration isolation and positioning platform. Part 2: experimental investigation and tests results. *Precis Eng* 2015; 40: 4.
5. Maggiore M, Broeck CD, Bartolo N, et al. Science case for the einstein telescope. *arXiv.org* 2020; 03. doi:10.1088/1475-7516/2020/03/050.
6. Wanner A, Bergmann G, Bertolini A, et al. Seismic attenuation system for the AEI 10 meter Prototype. *Class Quantum Gravity* 2012; 29: 245007.
7. Zhao G, Ding B, Watchi J, et al. Experimental study on active seismic isolation using interferometric inertial sensors. *Mech Syst Signal Process* 2020; 145: 106959.
8. Collette C, Janssens S, Fernandez-Carmona P, et al. Review: inertial sensors for low-frequency seismic vibration measurement. *Bull Seismol Soc Am* 2012; 102(4): 1289–1300.
9. Ding B. *Development of high resolution interferometric inertial sensors*. Université libre de Bruxelles, 2021.
10. Martin GD. *On the control of flexible mechanical systems*. Ph.D. Dissertation. Stanford University, 1978.
11. Jennifer W. *Active seismic isolation using interferometric inertial sensors*. Université libre de Bruxelles, 2022.
12. Skogestad S and Postlethwaite I. *Multivariable Feedback Control: Analysis and Design*. 2nd Edition. John Wiley & Sons, 2005, p. 592.
13. Hua W, Adhikari RX, DeBra D, et al. Low-frequency active vibration isolation for advanced LIGO. *Proc SPIE* 2004.
14. Köhlenbeck SM. *Towards the SQL interferometer length stabilization at the AEI 10 m-prototype*. PhD thesis. Gottfried wilhelm leibniz universität hannover, 2018.
15. Di Fronzo C. *Innovative perspectives for seismic isolation of gravitational-wave detectors*. PhD thesis. University of Birmingham, 2022.

Appendix

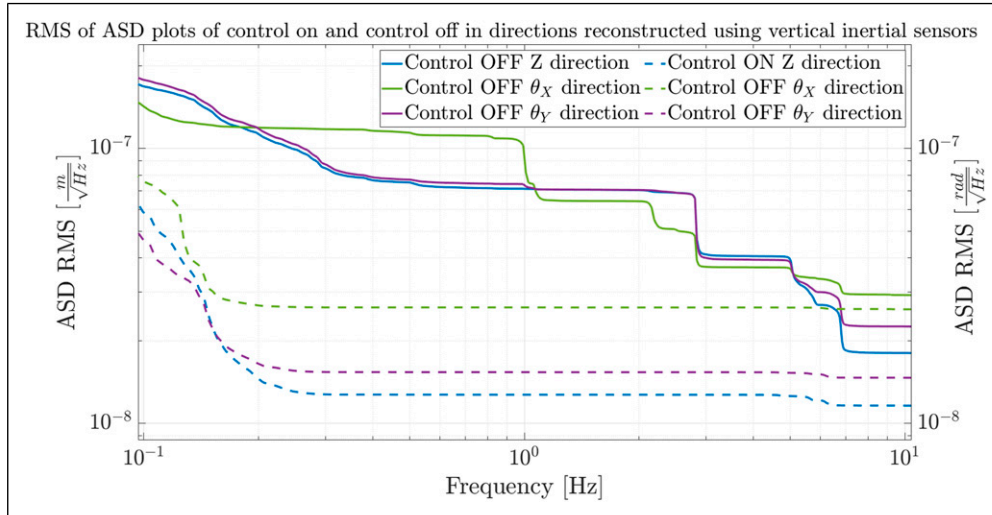


Figure 16. Cumulative RMS of amplitude spectral densities of displacements measured in Z, θ_X , and θ_Y directions on top of the platform for control off (solid lines) and control on (dashed lines).

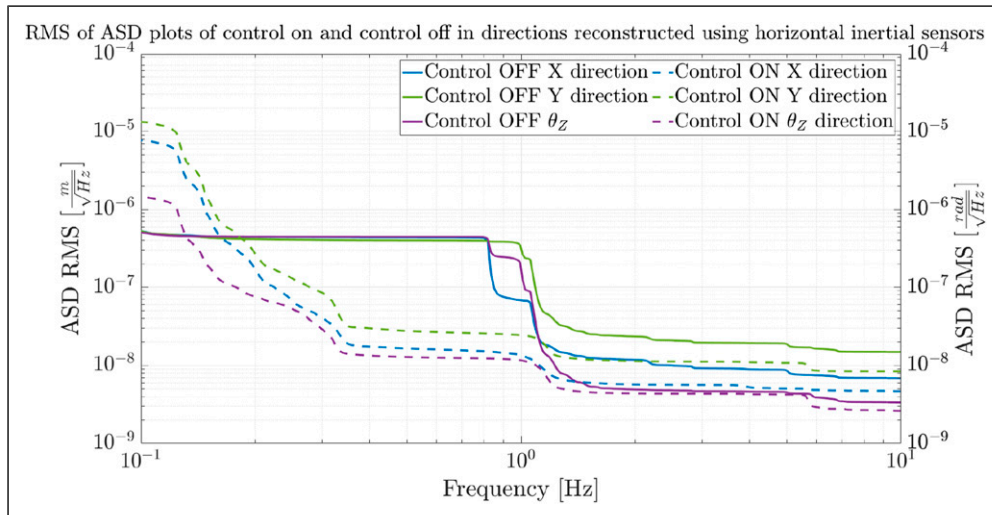


Figure 17. Cumulative RMS of amplitude spectral densities of displacements measured in X, Y, and θ_Z directions on top of the platform for control off (solid lines) and control on (dashed lines).